International Journal of Latest Research in Science and Technology **ISSN (Online):2278-5299**
Volume 3, Issue 1: Page No.14-19 ,January-February 2014
https://www.mnkpublication.com/journal/ijlrst/index.php

SHAPE-CONTROLLED DEPOSITION TEMPERATURES OF SINGLE-CRYSTALLINE $CdCO_3$ BY CHEMICAL BATH

[1]Ruth Melendrez Luevano,[2]Marcial Zamora Tototzintle,[3] M. Chávez Portillo, *[4]O. Portillo Moreno
[1,2,3,4]Lab. Materials Science, Facultad de Ciencias Químicas, Benemérita Universidad Autónoma de Puebla. Av, San Claudio y 14 Sur, Col. Sn. Manuel, P.O. Box 156, Puebla, Pue, 72001 México.

Abstract: - Different constant deposition temperatures (T_d) were employed in 20-80ºC to obtain CdS-$CdCO_3$thin films grown by Chemical Bath. By Scanning Electronic Microscopy for CdS-80 layer, it is observed that when the T_d decrease the morphology and size show change giving a variety of cube-shaped truncated cubes, wires and circles. With CdS-40 sample, the intensity of the x-ray Diffraction CdS peak is abruptly reduced.. The forbidden energy band gap was 2.4-4.1 eV. Raman spectra bands range 150-1800 cm^{-1} assigned to internal vibrations of CO_3^{2-} group: ν_1–symmetric stretching (1088 cm^{-1}) ν_3-asymmetric C-O stretching (1393 cm^{-1}); ν_4–in–plane band of the CO_3^{2-} (716 cm^{-1}); the first overtone A_{1g} + E_g (1772 cm^{-1}) and two bands assigned to translations and liberations' of the CO_3^{2-} group relative to the Cd atoms; ν_{13} (275 cm^{-1}), ν_{14} (165 cm^{-1}). In the range T_d 70-20°C lattice modes ν_{14} (165 cm^{-1}), ν_{13} (273 cm^{-1}), ν_3-asymmetric C-O stretching (1393 cm^{-1}), ν_1-symmetric C-O stretching 1088 cm^{-1}were observed.

Keywords **-** Deposition temperatures,Gibbs energy, coordination complex, grain size, electron affinity.

I. INTRODUCTION

The cadmium carbonate ($CdCO_3$: Octavite), and their physical properties, when mixed with CdS, have scarcely been studied. As such, can be useful in applications as insulators, composites, electrodes, sensors, among other devices. Octavite is a representative of carbonates with calcite type structure [1]. It is the principal natural resource for mining Cd, which finds its main application in the production of Ni-Cd batteries [2]. In the preparation of CdS or Cu(In, Ga)Se_2 thin films by chemical bath (CB), $CdCO_3$ is introduced as impurity into the semiconductor materials [4]. Structurally well-defined building blocks are potentially useful in the synthesis of designed catalysts, photonics band gap materials and chemical separations media [5]. A general approach to the fabrication in a precisely controlled manner is not yet available, but it is widely accepted that organic ligands or surfactants play a key role in determining not only the size but also the shape of the products [6]. We report the thermodynamic model by means of changes of Gibbs free energy in each stage to investigate the thermodynamic probability for the spontaneity of the reaction.

II.Chemical Reactions and experimental details

Scanning Electronic Microscopy (SEM) of the samples was recorded using a Hitachi (JEOL Model JSM6490) operating at an accelerating votage of 25 kV.Crystalline structure characterization was carried out by X-ray Diffraction (XRD) patterns registered in a Siemens D500 diffractometer, using the Cu $K_\alpha$line.The Raman spectra with a micro-Raman System Lab Ram-Idler with a line of 632.8 nm excitement. The OpticalAbsorption spectra, measured employing a Unicam 8700 Spectrometer, allowed us to calculate the E_g. The growth of the CdS is carried out according to the following stages: (*a*)By mixing $CdCl_2$, KOH, and NH_4NO_3, the coordination complex $[Cd(NH_3)_4]^{2+}$ is generated indirectly (*b*) The ions S^{2-}andCO_3^{2-} are found in the solution and are generated by thiourea.

II.1. CdS

The $S^{2-}$and CO_3^{2-} were generated from thiourea in alkaline medium

$$SC(NH_2)_2 + 3OH^- \Leftrightarrow CO_3^{2-} + S^{2-} + NH_4^+ + 3H^+ \quad (1)$$

$$S^{2-} + [Cd(NH_3)_4]^{2+} \Leftrightarrow CdS + 3NH_4^+ \quad (2)$$

ΔG^0 = - 135.19KJ

Like is observe$\Delta G^0 < 0$, therefore the reaction is spontaneous.

II.2.$CdCO_3$

$CdCO_3$ is generated gradually by reaction temeperature (T_d) on growth conditions of CdS [7,8,9]. The ions S^{2-} and CO_3^{2-} are generated from thiourea; they are solvable or insolvable in interval of T_d.

$Cd^{2+} + CO_3^{2-} \Leftrightarrow CdCO_3$ ΔG^o = - 65.247KJ (3)

Thermodynamic stability, solubility and reactivity of CO_3^{2-},Cd^{2+} and S^{2-} are related directly with parameter T_d, this is key in formation of CdS or $CdCO_3$

$CO_3^{2-} + CdS \Leftrightarrow CdCO_3 + S^{2-}$ ΔG^o = + 83.95KJ $T_d \leq 70$ºC (4)

Publication History
Manuscript Received : 27 January 2014
Manuscript Accepted : 31 January 2014
Revision Received : 2 February 2014
Manuscript Published : 28 February 2014

$$[Cd(NH_3)_4]^{2+} + CdCO_3 + 2S^{2-} \Leftrightarrow CO_3^{2-} + 2CdS + 3NH_4^+$$

$\Delta G^o = +6.95 KJT_d \geq 80^oC$ (5)

According with these results, as $\Delta G^o > 0$, the reaction (5) is not spontaneous.In the reaction the ions S^{2-} and CO_3^{2-} are generated from thiourea [9].

Preparation of crystalline thin films by CB on glass substrates at different deposition temperatures (T_d),$CdCl_2$ (0.02 M), KOH (0.5 M), NH_4NO_3 (1.5 M), and $SC(NH_2)_2$, (0.02 M) has been reported [7,9,10]. The relative concentrations, volume proportions, stirring, T_d, and pH were kept constant during the growth process [7,10]. The growing-time was since 15 min to 20 h.The samples were labeled CdS80, CdS70,…,CdS20 respectively.

III. Result and discussion

III.1.Scanning Electronic Microscopy (SEM)

The morphological analysis of the films was carried out in a SEM. Fig. 1 displays Micrographs low-magnification and high-magnification SEM images closely packed. These images show the morphology: CdS80-20 thin films, starting with theCdS-20. However it can be seen with CdS-70 that the products were cubes, when the T_d decrease the morphology and size of CdS show a change in a variety of cubes crystals including cubes-shaped truncated cubes, wires and circles. The closely packed microcrystals with flat surfaces and sharp edges/corner are clearly showed in the magnification SEM images. It is clearly seen that the large quantity of crystals have a smooth surface and almost all corner and edges of these cubes were slightly truncated. Inset of CdS-50 show the SEM image of slightly truncated cubes, indicating that the slightly truncated cubes are square/cube facets. These observations confirm that the CdS-20 circle consist of small crystals in perfectly aligned manners as found in many materials [11].

In addition, T_d is an important parameter in the formation of $CdCO_3$ cubes, circle and wires. Irregular particles $CdCO_3$were formed, the bigger cubes ~10-20 μm edge length were obtained. For CdS-20 film an interesting feature shown is that each ring comprises numerous particles aggregating on the surface. When the temperature of the building blocks (reactant species) of a solid becomes sufficiently high, that is, the solution is supersaturated. Supersaturation is a deterministic factor in the growth of the products [12] and T_d is also a deterministic factor in growth of $CdCO_3$. At this point, the crystals in suspension are colloidal and adhere to form agglomerates into small clusters (or nuclei) due their thermodynamic instability. With a continuous supply of building blocks, secondary growth processes such as Ostwald ripening or aggregation result in further growth to form larger circles, ring, and wires architectures [13].

The formed $CdCO_3$ crystallites possess different shapes and orientation facets, the combination probability on the succeeding crystallites will depend on the surface energies and structures of the crystallites; that is to say, a suitable structure of the crystal is critical for the intergrowth of $CdCO_3$. Generally, only the microcrystals with same or similar shapes attach together. With more and more cubes attaching to the existent $CdCO_3$ one by one in the same way, a chain-like structure is formed. Therefore, $CdCO_3$ wires, circles, are formed by oriented aggregation mechanism [14]. For CdS-80, polycrystalline films were formed, observation of the films shows smooth surface and well adhesive nature of the films with substrate, however for CdS-70, it is showed that the growth of grain $CdCO_3$ distributed across the surface of the film CdS.

The size grain of microcrystalline material show structure (they look cubic at first glance). This abrupt transition in a crystal size and morphology occurs with decrease T_d suggesting a change in the deposition and also results in the deposition mechanics, further decrease in T_d result in complete transition to faceted regular. The assembly of anisotropic nanostructures, including nanotubes and nanowires, requires more effort and remains a good challenge. Fortunately, recent progress demonstrated the good manipulation on the assembly of these more complex structures, including nanorods and nanowires. The alignment of nanowires made of silver nanoparticles was demonstrated using a Langmuir-Tough by Heat and co-workers [15].

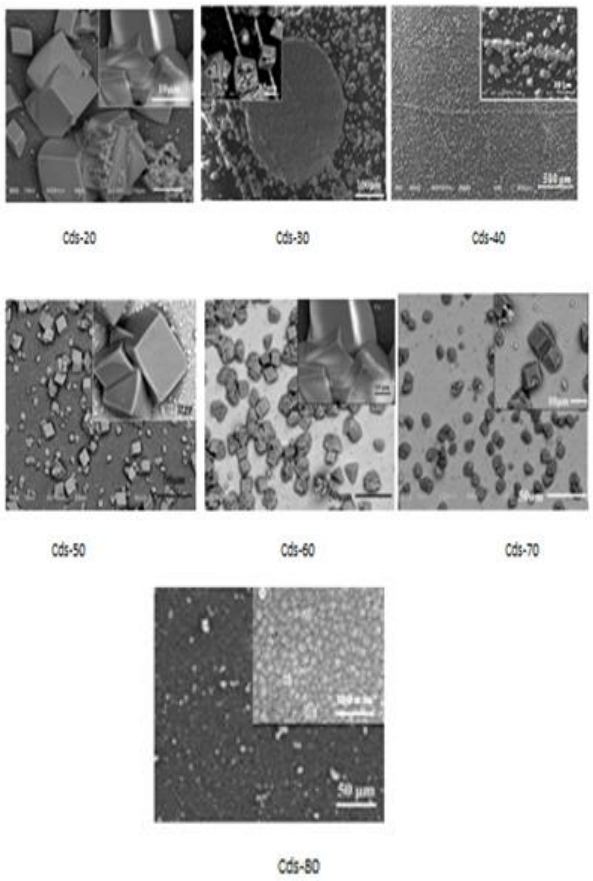

Figure 1. Micrographs with high- and low-magnification SEM images closely packed. These images show the morphology of CdS20-80 layers.

Ordered chains of $BaCrO_4$ were observed and assembly of these structures was attributed to interactions between the surfactants on surface of the adjacent nanorods [15], Nikoobakht and co-workers suggested that in the assembly of nanorods, the interacting forces determining the parallel alignment between nanorods include higher lateral capillary forces along the length of the nanorod than its width, and van der Waals attraction and a screened Coulomb repulsion between nanorods [16]. Yang and co-workers adopted the technique of Langmuir-Blodgett assembly of monolayers to assemble and align $BaCrO_4$ and $BaWO_4$ nanorods [17]. They not only demonstrated the ordered side-by-side alignment of these nanorods but also found singularity structures in assembly of multilayered nanorods structures, which was also found by Alivisatos and co-workers in the assembly of CdSe nanorods [18]. Besides the directional capillarity force and van der Waals attraction as mentioned above, the consideration that the maximization of the entropy of the self-assembled structures by minimizing the excluded volume per particle in array by Onsager was also taken into account in their explanation [18].

III.2. X-ray Diffraction (XRD)

XRD CdS80-20patterns are illustrated in Fig.2. The CdS-80sample displays the hexagonal Wurzite (WZ) crystalline phase as dominant structure. The two small peaks at both sides of (002) central reflection define the triplet that distinguishes at hexagonal phase from cubic zinc blende (ZB) structure in CdS [JDPDS-ICDD X-ray-cards10-454 and 6-314].For CdS-70, the XRD maximum peak is also located at 2θ= (26.5), two small peaks at both sides of (002), other small XRD lines begin to appear at 2θ = 23.5° and 30.3°. The sample with CdS-20the XRD peaks at 2θ = (23.4,30.2,36.4, 40.1, 43.8, 48.0, 49.5, 49.9, 58.2, 61.7, 62.9, 65.5)all reflections were indexed by assigning them octavite which has rhombohedral crystalline structure [JCPDS 042-1342]. The absence of CdS peaks in the pattern of CdS-20 may indicate that CdS has been dispersed into the structure of $CdCO_3$.

In addition, the XRD revealed than the cube-like structured $CdCO_3$ crystals tend to grow preferentially along (012) and (104) direction. As T_d goes down, the crystalline structure of layers gradually shows a larger contribution of XRD-$CdCO_3$ peak, with the respective diminution in intensity of XRD-CdS lines. In CdS- 60 and CdS50 samples, the intensities located in angular position: 2θ = (23.4, 26.5, 30.2, 33.4, 36.5, 44.1, 43.8, 49.5) that indicate co-existence of one solid solution of CdS-$CdCO_3$. According to patterns XRD CdS-30 toCdS-20 range, are located the transition CdS→$CdCO_3$.

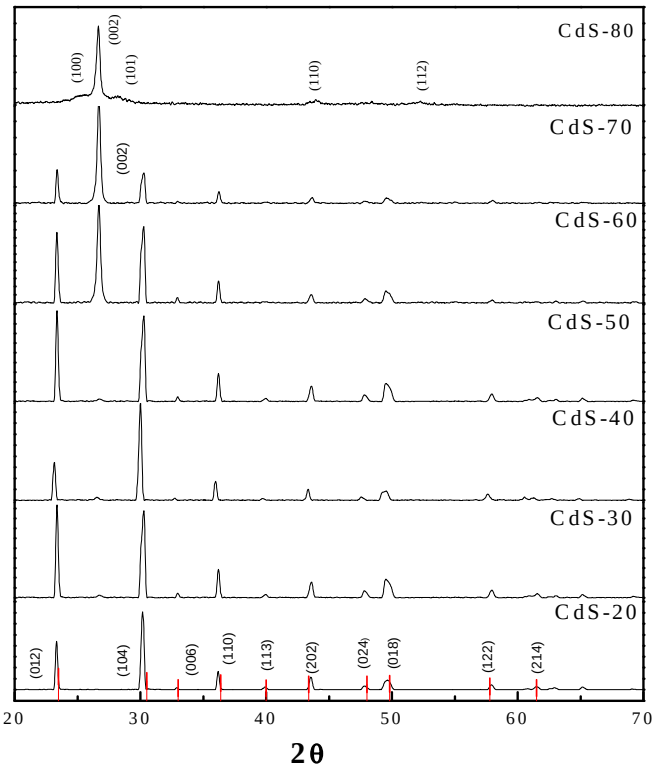

Figure 2. X-ray diffraction patterns of CdS20-80 layers, for different temperature deposition.

III.3. X-ray Diffraction (XRD)

Assuming parabolic band structure, the absorption coefficient α is proportional to

$$(E - E_g)^{\frac{1}{2}} = \alpha h\gamma$$

And an extrapolation to $\alpha^2 = 0$ yields isa good approximation of band gap (E_g). With this technique it is possible to plot the percentage (%) of the transmittance (T).Optical absorption spectra allow to calculate E_g for all the films. The transmission spectra in the wave range 200-800 nm of layers are shown in Fig.3. This show a shift of their transmission edges to low wavelength and also show a shift to their transmission edges towards high energies. Films CdS-60 had better optical quality, which is evident from sharp fall in transmission at the absorption edge, indicating better crystallinity of the films.

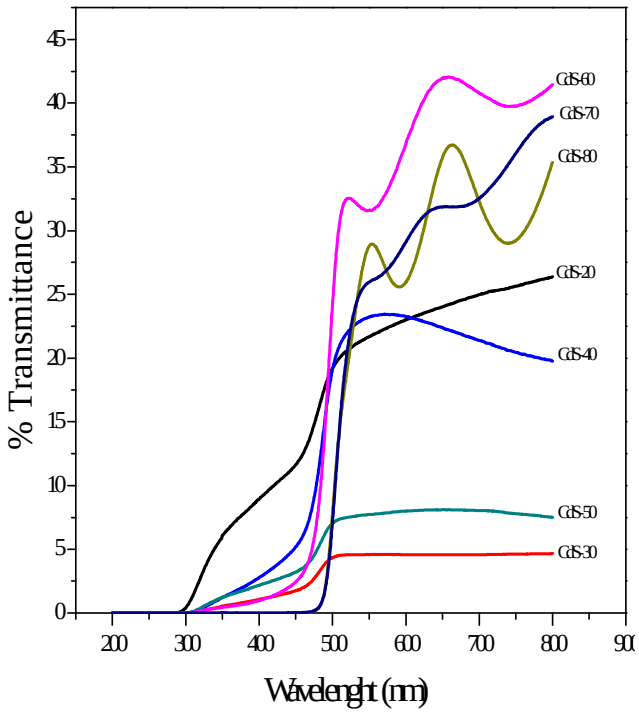

Figure 3. The optical transmittance CdS80-20 films.

The absorbance is very small and the transmission 80%, which indicates that the sample has a minimum impurity and lattice defects. The paralled transmission shift however indicates that there are related to changes in films structure. The increase in transmittance with increase in UV region is not sharp. This fact indicates that the absorption band gap transition in the films are due to direct transitions. Films formed on the surface at lower temperature CdS-50 and CdS-30 have less transmision due to the $CdCO_3$ formation on the surface of CdS, which reduces the optical transmission.

The parallel transmission shift however indicates that it is related to changes in structure [19].According to DRX spectraand the optical absorption, the transition CdS→$CdCO_3$ inCdS-20 to CdS-30is confirmed, however there small amountsof CdS.Figure 4 exhibits $(\alpha^2 h\nu)^2$versus hν plot for CdS80-20 films.

The extrapolation of the linear part of curve intercepts the $h\nu$-axis. In the inset, the same procedure is illustrated for the E_g values CdS-30 and CdS-20°C samples. By the difference in the range of 2.5-4.1 eV, the graphic is placed in the inset for CdS-20 and CdS-30 films respectively. The region where the curve is a straight line and its extrapolation until the energy for the determination of E_g in the films of $CdCO_3$ and CdS, and in its inset, respectively are clearly defined. However for sample CdS-60, whose fitting for E_g determination are despicted in Fig. 4 the linear region for extrapolation is non unique. According with the inset of this Fig. at CdS-60, for instance, two linear parts can be extrapolated in two values of direct E_g are defined. All this behaviour is an indication that for CdS-60°C, both materials are aggregated one from the another one.

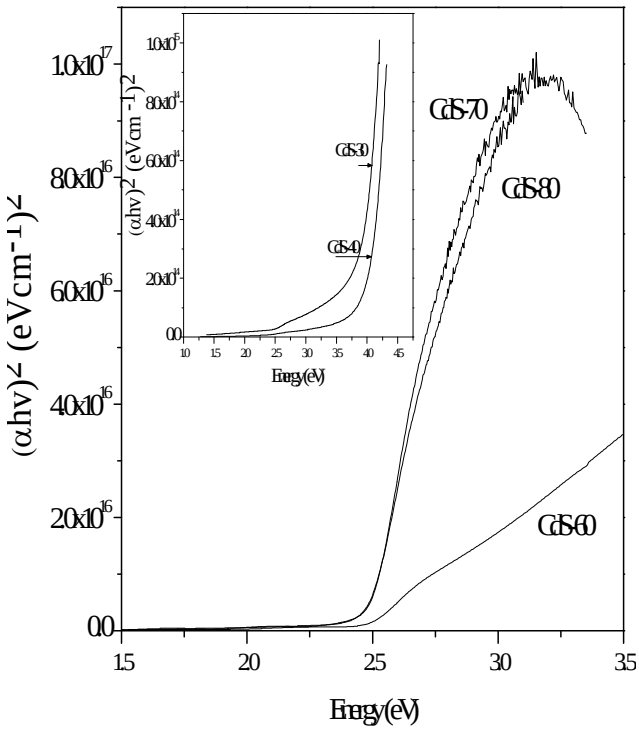

Figure 4. $(\alpha^2 h\nu)^2$versus $h\nu$ plot for CdS80-60, films. The inset show that the layerCdS-40, CdS-30 films respectively.

These spectra exhibit different features depending on the morphological variation, the absorption spectra of CdS-$CdCO_3$ properties of crystals are generally impacted by many factors, such as particle shape, size, and size distribution. In particular, the effect of lattice defect could be ignored. It is considered that the cubes with longer crystalline have low concentration of defects, which act at sites for nonradiatives recombination of electron-hole pair.

Another particularity observed in Figure 4 is the presence of band-tail absorption. This phenomenon is due to the existence of a tail density if gap state in degenerate materials, which has been attributed to local mechanical stress produced by impurities exhibits and exponential dependence on photon energy $\alpha = ke^{\frac{E}{E_0}}$, being a characteristic increases with impurity concentration.

III.4, Raman spectroscopy

The 632.8 nm wavelength laser Raman spectroscopy was used to analyze films. The peaks observed at 252 cm^{-1} is E_2, 228 cm^{-1} A_1(TO), 235 cm^{-1} E_1(TO), 305 cm^{-1} E_1(LO) and A_1(LO) respectively, of Wurzite (WZ) CdS [32]. The peaks observed at 305 cm^{-1} is ILO, 246 cm^{-1} TO, 610 cm^{-1} 2LO of zinc blende (ZB) of CdS. However, the peak observed at 246 cm^{-1} is attributed to a shift in either the transverse optical (TO)peak of ZB CdS [20] or the E_1(TO) peak of WZ CdS.The resonance Raman spectra ofCdS-80,CdS-70,…,CdS-20 fims, from 100 to 1500 cm^{-1} is shown in Fig.5. Raman spectra of the CdS-80 film consists of three different peaks at 223,309 and 606 cm^{-1}, CdS characteristic peaks E_2,

E_1(TO) and ILO attributed to WZ phase [20], is barely noticeable at about 600 cm^{-1}.The prominent peak at 309 cm^{-1} is attributed to either the ZB 1LO phonon or the WZ A_1(LO)/E_1(LO) phonons [21].

In our work, however, this peak is observed at 309 cm^{-1} rather than at 274 cm^{-1}, which may be attributed to the TO phonon of ZB CdS rather than the E_1(TO) peak of hexagonal CdS [22]. Peaks were detected for the A_1(TO) phonon of WZ CdS. E_1(LO), E_1(TO) and E_2 phonons for W single crystal CdS as well as values of 1LO, 2LO, and TO phonons for ZB CdS. Another CdS characteristic peak, longitudinal optical (LO) [35], is barely noticeable at about 600 cm^{-1}. The peak observed for annealing films was at 276 cm^{-1} [23], and it is ruled out TO phonon possibility an attributed this peak to shift in the E_1(TO) peak WZ CdS, this peak is observed at 276 cm^{-1} but however in our work this peak is observed at 274 cm^{-1}, which may be attributed to the phonon of ZB CdS rather E_1(TO) than hexagonal phase. A closer look at the main peak at 310 cm^{-1} shows the peak being asymmetric, suggesting a superposition of more than one mode. A closer look at the main peak 310 cm^{-1} shows the peak being asymmetric, suggesting a superposition of more than one mode. The Raman spectrum $CdCO_3$ at ambient conditions is well-known[24]. A symmetry analysis showed that five Raman active bands for $CdCO_3$ [$1A_{1g}(\nu_1)$, $4E_g$ (ν_3,ν_4,ν_{13}, ν_{14})] are allowed.

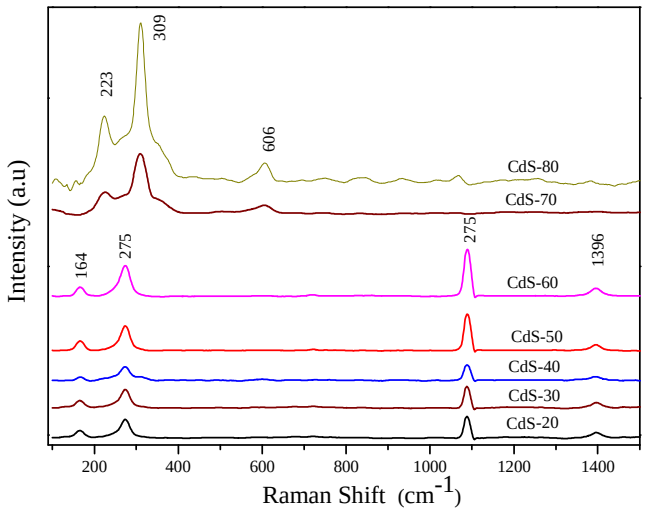

Figure 5 .Raman spectra of CdS80-20 samples, lattice modes ν_{14} (165 cm^{-1}),ν_{13} (275 cm^{-1}),ν_4–in–plane band of theCO_3^{2-}(716 cm^{-1}),ν_3 -asymmetric C-O stretching (1393 cm^{-1}), ν_1-symmetric C-O stretching 1088 cm^{-1}.

Lattice modes ν_{14} (165 cm^{-1}), ν_{13} (273 cm^{-1}), ν_3-asymmetric C-O stretching (1393 cm^{-1}), ν_1-symetric C-O stretching 1088 cm^{-1}. The intensity of the ν_{14} band, associated with lattice vibration parallel to the *c*-axis. We observe four bands in the frequency range 150-1800 cm^{-1} assigned to internal vibrations of CO_3^{2-} group: ν_1–symetric stretching (1088 cm^{-1}) ν_3-asymetric C-O stretching (1393 cm^{-1}); ν_4– in–plane band of the CO_3^{2-} (716 cm^{-1}); the first overtone A_{1g} + E_g (1772 cm^{-1}) and two bands assigned to translations and liberations' of the CO_3^{2-} group relative to the Cd atoms; ν_{13} (275 cm^{-1}), ν_{14} (165 cm^{-1}). The behavior of the bands with variation CdS- 60 is very similar. An increase of the intensity in all of the Raman bands with both the increase in T_d.

IV. CONCLUSIONS

Preparation of crystalline CdS-$CdCO_3$ thin films was performed at deposition temperatures (T_d) in 20-80ºC range by CB. T_d is an important parameter in the formation $CdCO_3$ cubes, circle and wires. Crystallites with different shapes and orientation facetsalong with the combination probability on the succeeding crystallites will depend on the surface energies and structures of the crystallites.XRD peaks at 2θ = (23.4, 30.2, 36.4, 40.1, 43.8, 48.0, 49.5, 49.9, 58.2, 61.7, 62.9, 65.5) for CdS-20sample all reflections were indexed by assigning them octavite which has rhombohedracrystalline structure. We observed four bands in the frequency range 150-1800 cm^{-1} assigned to internal vibrations of CO_3^{2-} group: ν_1–symmetric stretching (1088 cm^{-1}) ν_3-asymmetric C-O stretching (1393 cm^{-1}); ν_4– in–plane band of the CO_3^{2-} (716 cm^{-1}); the first overtone A_{1g} + E_g (1772 cm^{-1}) and two bands assigned to translations and liberations' of the CO_3^{2-} group relative to the Cd atoms; ν_{13} (275 cm^{-1}), ν_{14} (165 cm^{-1}).

References

[1] D. L. Graf, Am. Mineralogitic, 46 (1961) 1283-1319.

[2] R. E. Kirk, D. F. Othmer, A. Seidel, Vol. 2, 5 ed., Wiley-interscience, Hoboken, N J 2007.

[3] L. Borodin, V. I. Lyutin, V. V. I. Iykhin, V. V. Belov, Doklady Akademii Nauk SSSR 245 (1979) 1099-1101.

[4] Kylner, J. Lindgren and L Stolt, Electrochem. Soc. 143 (1996) 2662-2669.

[5] Geoffrey A. Ozin, Adv. Mater. 4 (1992) 612-622.

[6] Y. Yin, A. P. Alivisatos, Nature 437 (2005) 664-670.

[7] O. Portillo Moreno, H. Lima Lima, R. Lozada Morales, R. Palomino Merino, O. Zelaya Ángel, J. of Mat. Sci.40 (2005) 1-4.

[8] J. Bethune and N.A.S: Loud, "Standard Aqueous Potential and Temperature Coefficients at 25ªC", C. A. Hampel, Skokie, III, 1964.

[9] O. Portillo Moreno, H. Lima Lima, V. Ramirez Falcón, J. Martínez Juárez, G. Juárez Diaz, R. Lozada Morales, R. Rebollo Plata, R. Palomino Merino, A. B. Soto Guzmán, O. Zelaya Ángel, J. of Electrochem. Soc. 153 (2006) 926-930.

[10] O. Portillo Moreno, G. Abarca Ávila, J. R. Cerna, J. Hernández Tecorralco, M. Chávez Portillo, J. Martínez Juárez, R. Lozada Morales, O. Zelaya Ángel, J. of Mat. Sci. and Engin.A 1 (2010) 692-704.

[11] S. Ashoka, G. Nagaraju, K. V. Thipperudraiah, G. T. Chandrappa, Mat. Res. Bull.45 (2010) 1736-1740.

[12] T. Jung, W. S. Kim, C. K. Choi, Cryst. Res. Nanotechology 17 (2006) 5686.

[13] Culling Gao, Wenli Zhang, HongbianLi, Leibing Lang, and Zheng Xu, Cryst. Growth, Des. 8 (2008) 3785-3790.

[14] C. M. Wuang, Y. Cheng, Y. S. Wang, F. Bao, Chin J. Struct. 26 (2007) 757.

[15] Nikoobakht, B.; Wang, Z. L.; El Sayed, M. A.J. Phys. Chem. B 104 (2000) 8635-8640.

[16] F.Kim. S.Kwan, J.Akana, P.Yang, J. Am. Chem. Soc. 123 (2001) 4360.

[17] Peidong Yang and Franklin Kim. Chem. Phys. Chem. 3 (2002) 503-506.

[18] Li, L. S.; Alivisatos, A. P. Adv. Mater 15 (2003) 408-411.

[19] J. P.Neufville, S. C. Moss, and S. R. Ovshinky,J. Non. Cryst. Solids 13 (1993) 191223.

[20] Nusimovici, M. A.; Birman, J. L. Phys. Rev. 156 (1967) 925.

[21] M. Froment, M. C. Bernard, R. Cortes, B. Mokili, D. Lincot, J. Electrochem. Soc. 142 (1995) 2624.

[22] W. B. Withe, (Ed.: V. C. Farmer), Mineralogical, London, 1974, pp. 227-279.

[23] R. C. C. Leite, S. P. S, Porto, Phys. Rev. 17 (1966) 10-12.

[24] Tell B, Damen T and Porto S Phys. Rev. 144(1966) 77.

[25] H. N. Rutt, J. H. Nicola, J. Phys. C: Solid State Phys. 7 (1974) 4522-4228